Persistent Atmospheric Carbon Dioxide Biases in Earth System Models and Community Research Directions

Forrest M. Hoffman, James T. Randerson, Vivek K. Arora, Qing Bao, Patricia Cadule, Duoying Ji, Chris D. Jones, Michio Kawamiya, Samar Khatiwala, Keith Lindsay, Atsushi Obata, Elena Shevliakova, Katharina D. Six, Jerry F. Tjiputra, Evgeny M. Volodin, Tongwen Wu

DOE Integrated Climate Modeling Principal Investigator (PI) Meeting

May 13, 2014

U.S. DEPARTMENT OF ENERGY

UCIRVINE

UCI DEPARTMENT OF EARTH SYSTEM SCIENCE

Climate Change Science Institute
AT OAK RIDGE NATIONAL LABORATORY

OAK RIDGE NATIONAL LABORATORY
MANAGED BY UT-BATTELLE FOR THE U.S. DEPARTMENT OF ENERGY

Research Questions

Question 1

How well do Earth System Models (ESMs) simulate the observed distribution of anthropogenic carbon in atmosphere, ocean, and land reservoirs?

Research Questions

Question 1

How well do Earth System Models (ESMs) simulate the observed distribution of anthropogenic carbon in atmosphere, ocean, and land reservoirs?

Question 2

Can we use contemporary atmospheric CO_2 observations to constrain future CO_2 projections?

Observed Carbon Accumulation Since 1850

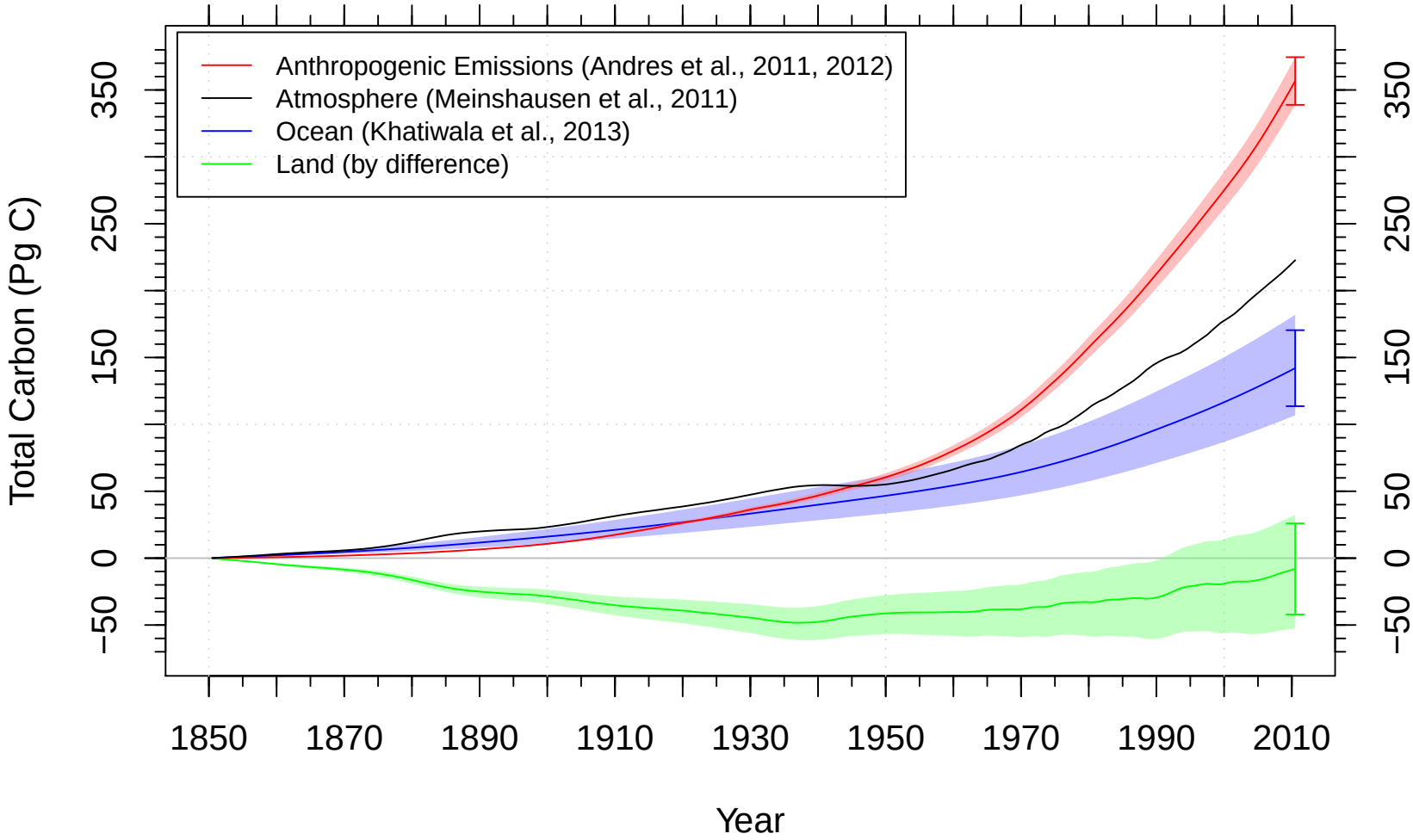

Observational estimates of anthropogenic carbon inventories in atmosphere, ocean, and land reservoirs for 1850–2010. Atmosphere carbon is a fusion of Law Dome ice core CO_2 observations, the Keeling Mauna Loa record, and more recently the NOAA GMD global surface average, integrated for the purpose of forcing IPCC models. Total land flux is computed by mass balance as follows:

$$\Delta C_L = \sum_i F_i - \Delta C_A - \Delta C_O.$$

15 fully-prognostic ESMs that performed CMIP5 emissions-forced simulations

Model	Modeling Center
BCC-CSM1.1	Beijing Climate Center, China Meteorological Administration, CHINA
BCC-CSM1.1(m)	Beijing Climate Center, China Meteorological Administration, CHINA
BNU-ESM	Beijing Normal University, CHINA
CanESM2	Canadian Centre for Climate Modelling and Analysis, CANADA
CESM1-BGC	Community Earth System Model Contributors, NSF-DOE-NCAR, USA
FGOALS-s2.0	LASG, Institute of Atmospheric Physics, CAS, CHINA
GFDL-ESM2g	NOAA Geophysical Fluid Dynamics Laboratory, USA
GFDL-ESM2m	NOAA Geophysical Fluid Dynamics Laboratory, USA
HadGEM2-ES	Met Office Hadley Centre, UNITED KINGDOM
INM-CM4	Institute for Numerical Mathematics, RUSSIA
IPSL-CM5A-LR	Institut Pierre-Simon Laplace, FRANCE
MIROC-ESM	Japan Agency for Marine-Earth Science and Technology, Atmosphere and Ocean Research Institute (University of Tokyo), and National Institute for Environmental Studies, JAPAN
MPI-ESM-LR	Max Planck Institute for Meteorology, GERMANY
MRI-ESM1	Meteorological Research Institute, JAPAN
NorESM1-ME	Norwegian Climate Centre, NORWAY

CMIP5 Long-Term Experiments

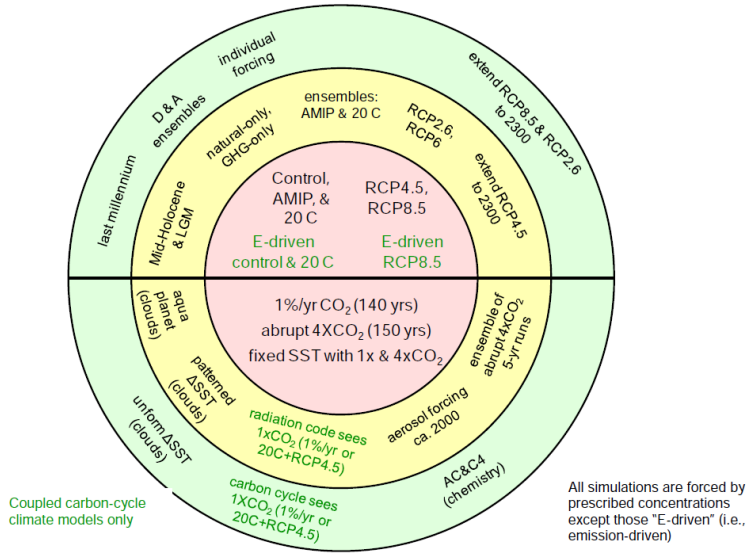

Emissions for Historical + RCP 8.5 Simulations

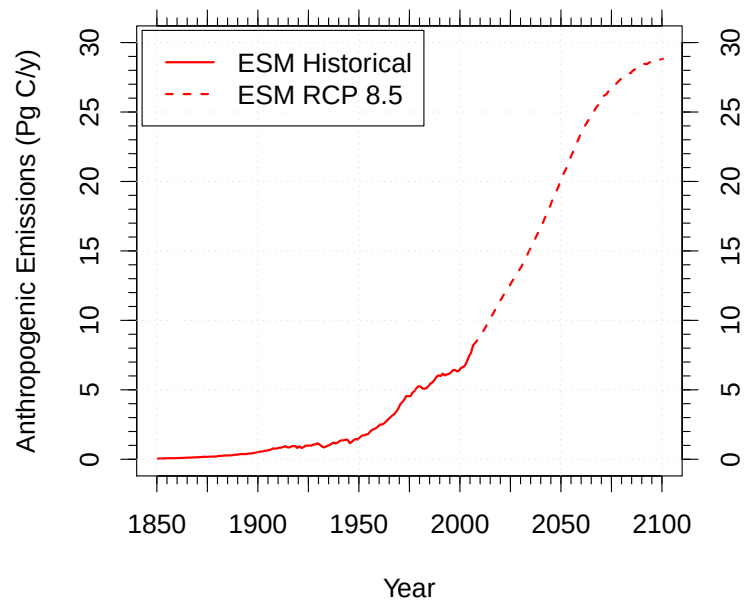

(a) Most ESMs exhibit a high bias in predicted atmospheric CO_2 mole fraction, which ranges from 357–405 ppm at the end of the historical period (1850–2005).

(b) The multi-model mean is biased high from 1946 throughout the 20th century, ending 5.6 ppm above the observed value of 378.8 ppm in 2005.

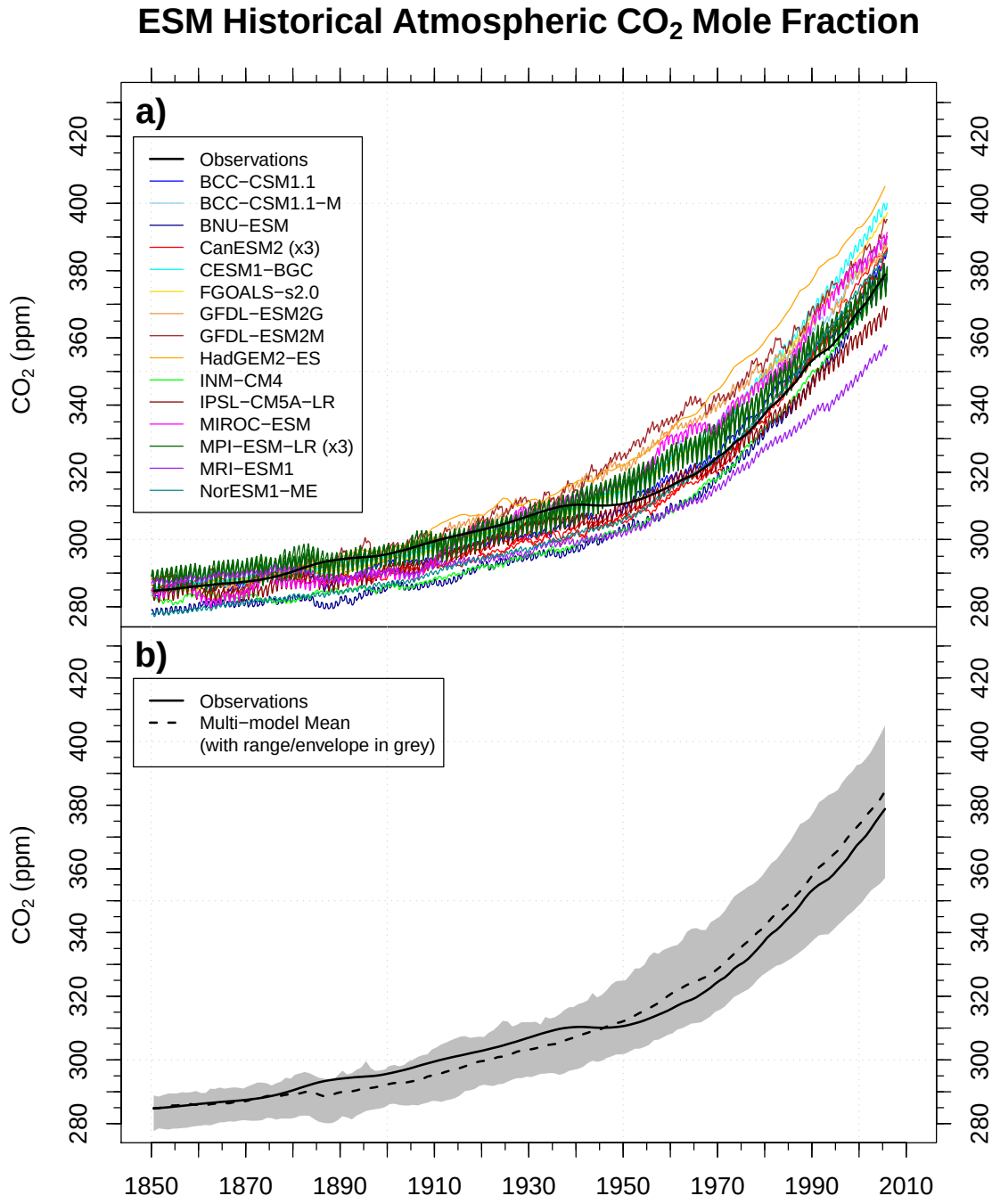

(Hoffman et al., 2014)

Model inventory comparison with Khatiwala et al. (2013)

Once normalized by their atmospheric carbon inventories, most ESMs exhibit a low bias in anthropogenic ocean carbon accumulation through 2010.

The same pattern holds for the Sabine et al. (2004) inventory derived using the ΔC^* separation technique.

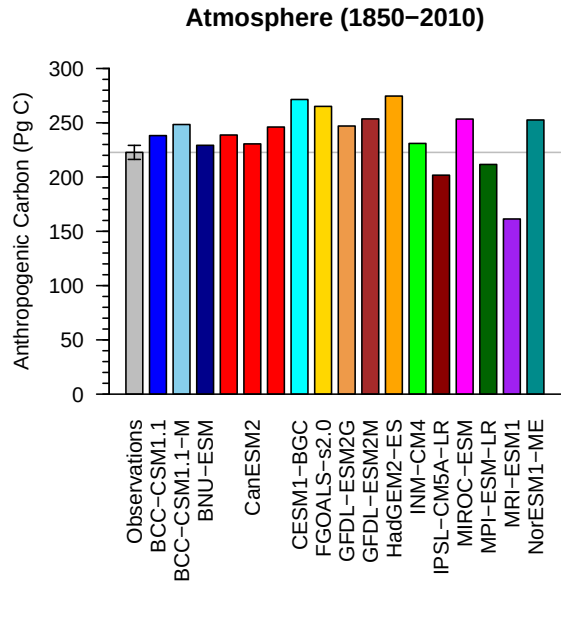

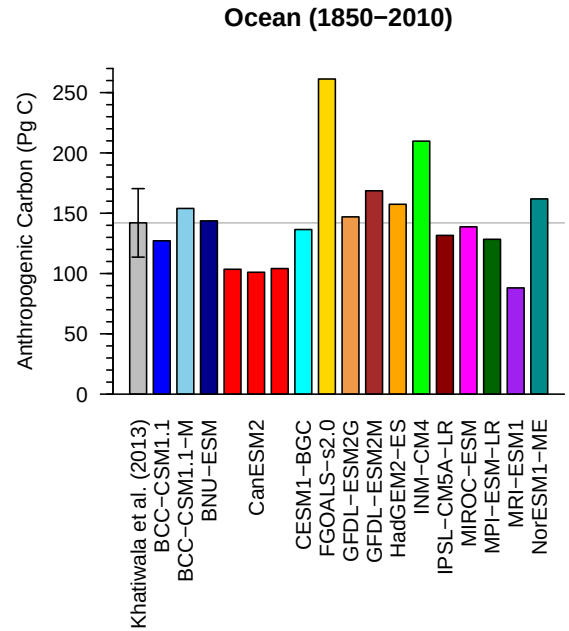

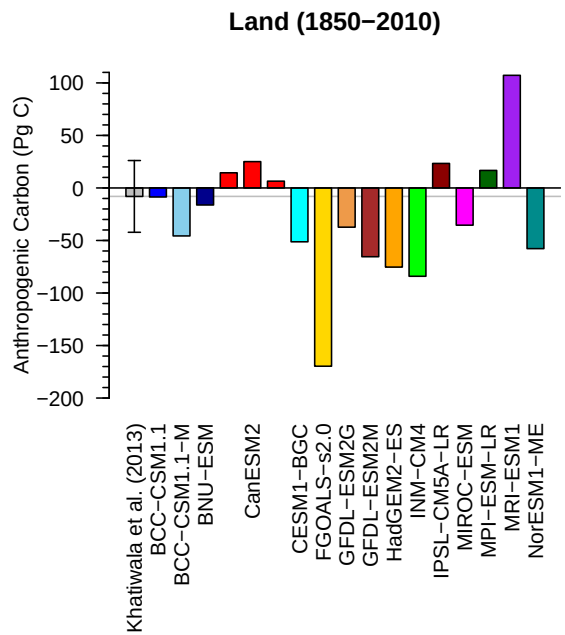

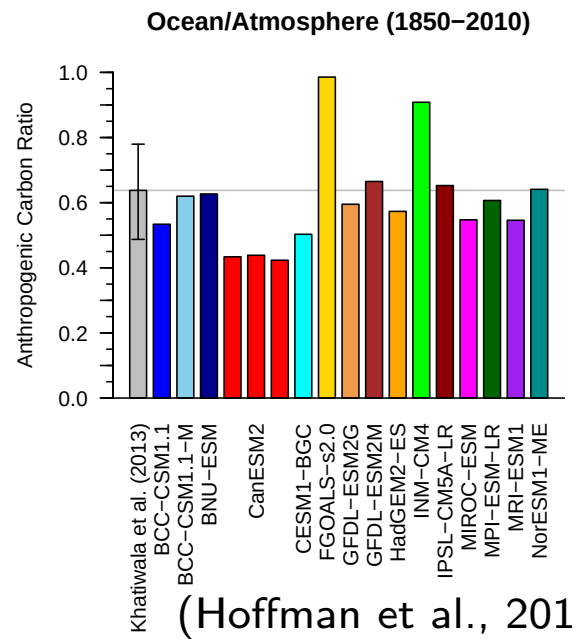

(Hoffman et al., 2014)

(a) Ocean inventory estimates have a fairly persistent ordering during the second half of the 20th century.

(b) ESMs have a wide range of land carbon accumulation responses to increasing CO_2 and land use change, ranging from a net source of 170 Pg C to a sink of 107 Pg C in 2010.

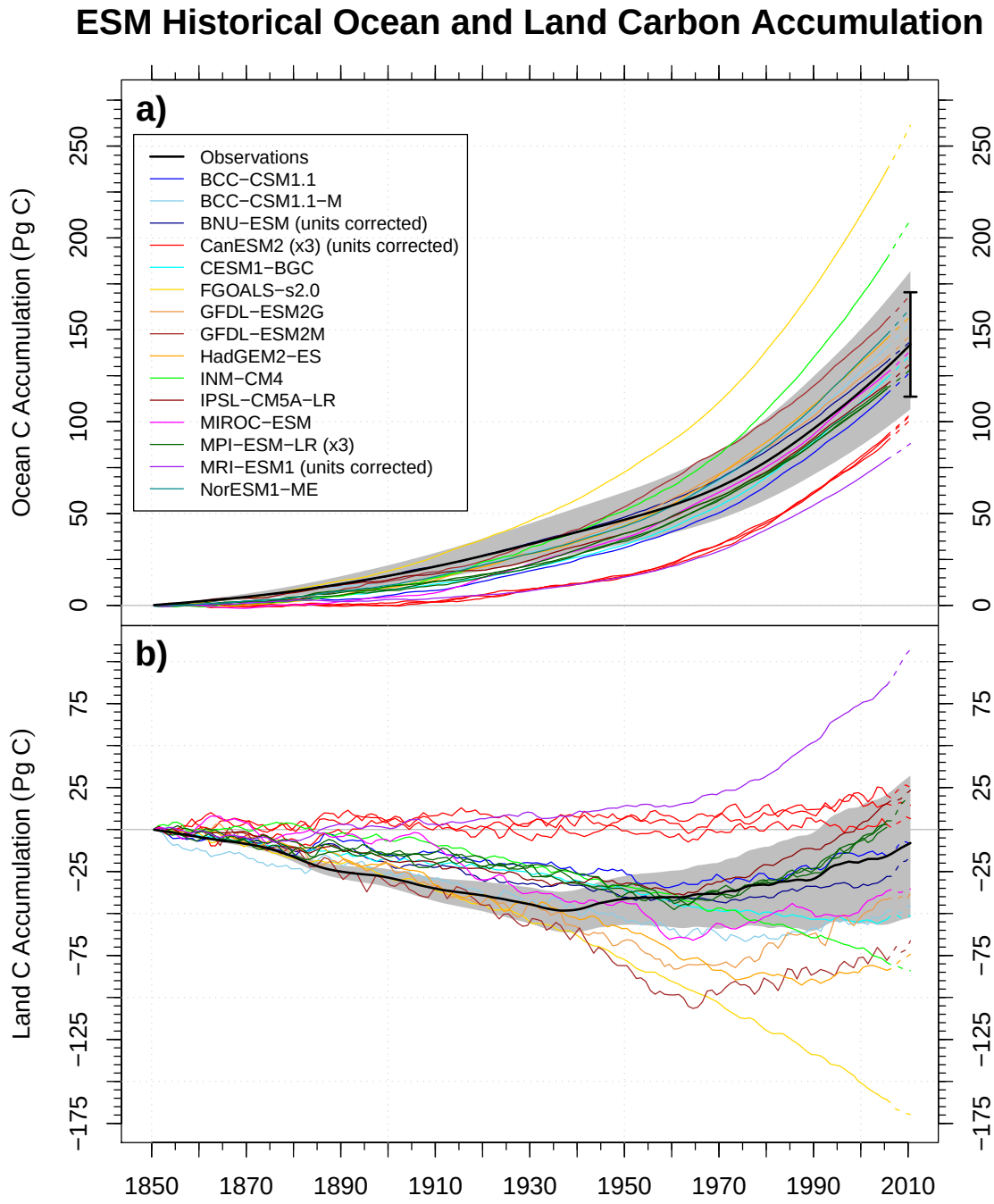

(Hoffman et al., 2014)

Question 2

Can we use contemporary atmospheric CO_2 observations to constrain future CO_2 projections?

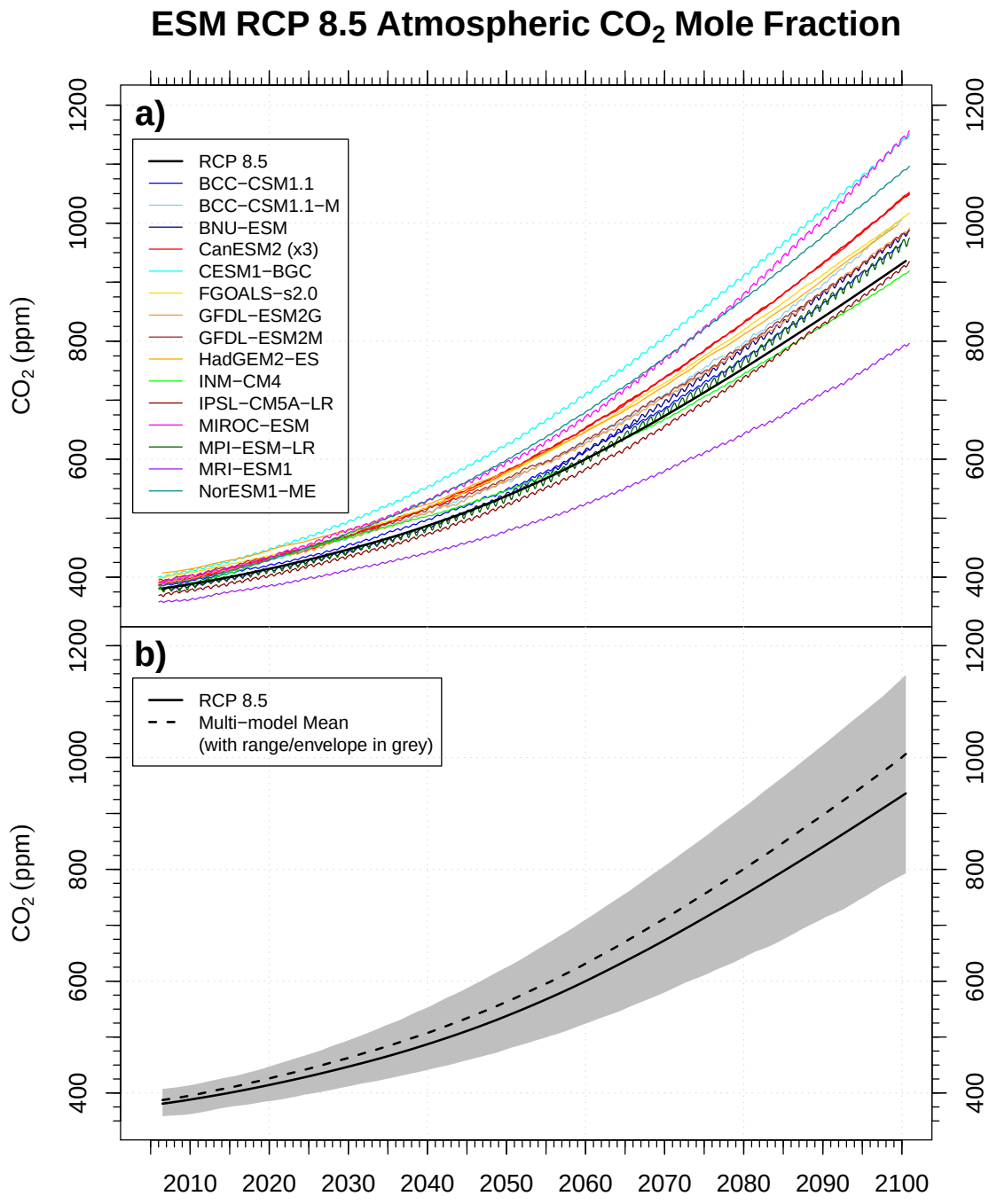

(Hoffman et al., 2014)

Reducing Uncertainties Using Observations

To reduce feedback uncertainties using contemporary observations,

1. there must be a relationship between contemporary variability and future trends on longer time scales within the model, and

Reducing Uncertainties Using Observations

To reduce feedback uncertainties using contemporary observations,

1. there must be a relationship between contemporary variability and future trends on longer time scales within the model, and
2. it must be possible to constrain contemporary variability in the model using observations.

Reducing Uncertainties Using Observations

To reduce feedback uncertainties using contemporary observations,

1. there must be a relationship between contemporary variability and future trends on longer time scales within the model, and
2. it must be possible to constrain contemporary variability in the model using observations.

Example #1

Hall and Qu (2006) evaluated the strength of the springtime snow albedo feedback (SAF; $\Delta\alpha_s/\Delta T_s$) from 17 models used for the IPCC AR4 and compared them with the observed springtime SAF from ISCCP and ERA-40 reanalysis.

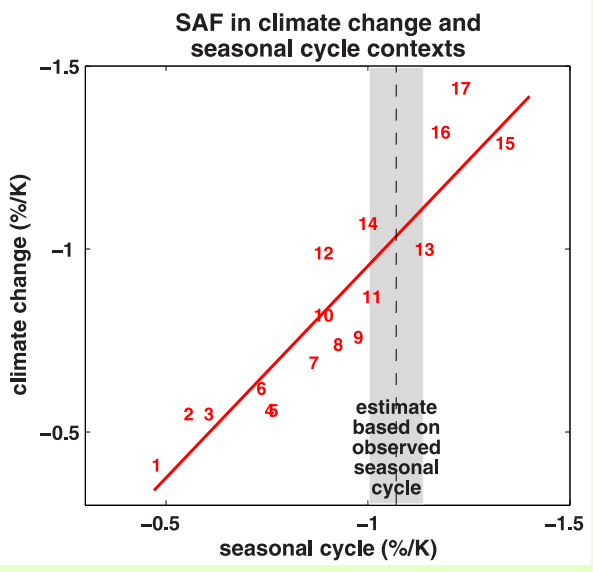

Reducing Uncertainties Using Observations

To reduce feedback uncertainties using contemporary observations,

1. there must be a relationship between contemporary variability and future trends on longer time scales within the model, and
2. it must be possible to constrain contemporary variability in the model using observations.

Example #2

Cox et al. (2013) used the observed relationship between the CO_2 growth rate and tropical temperature as a constraint to reduce uncertainty in the land carbon storage sensitivity to climate change (γ_L) in the tropics using C^4MIP models.

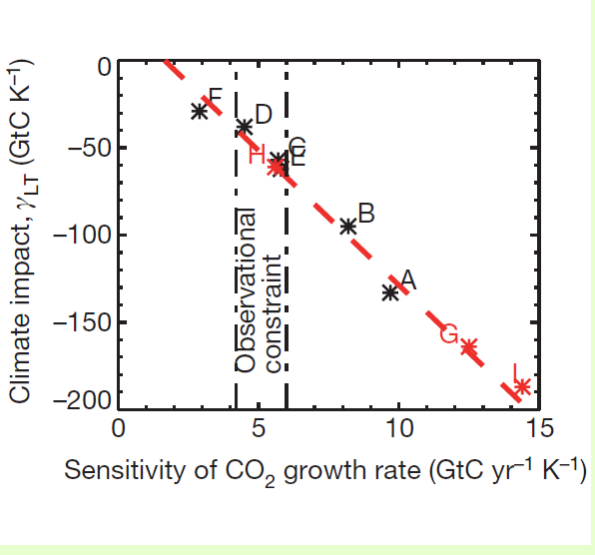

We developed a new emergent constraint from carbon inventories.

A relationship exists between contemporary and future atmospheric CO_2 levels over decadal time scales because carbon model biases persist over decadal time scales.

Observed contemporary atmospheric CO_2 mole fraction is represented by the vertical line at 384.6 ± 0.5 ppm.

(Hoffman et al., 2014)

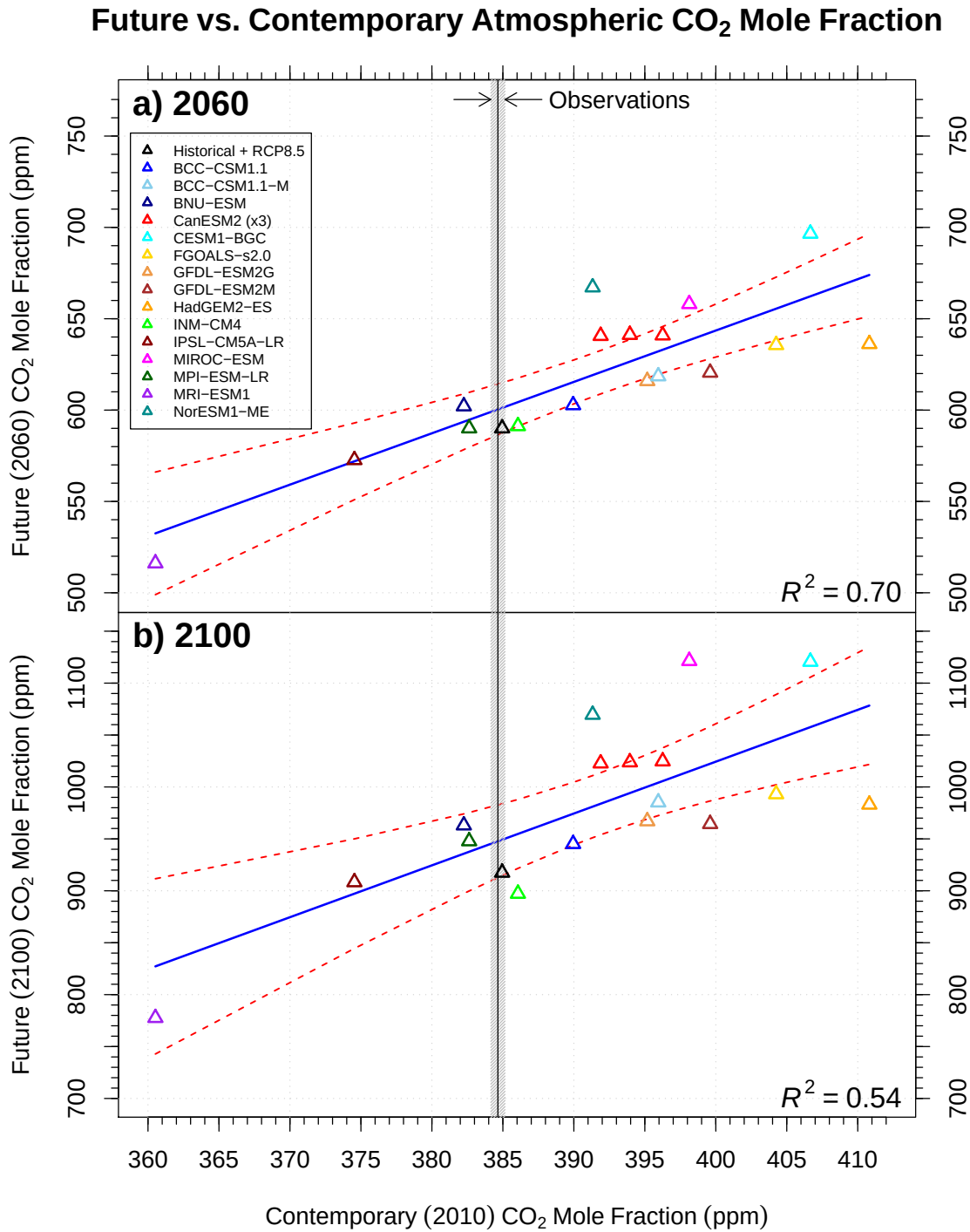

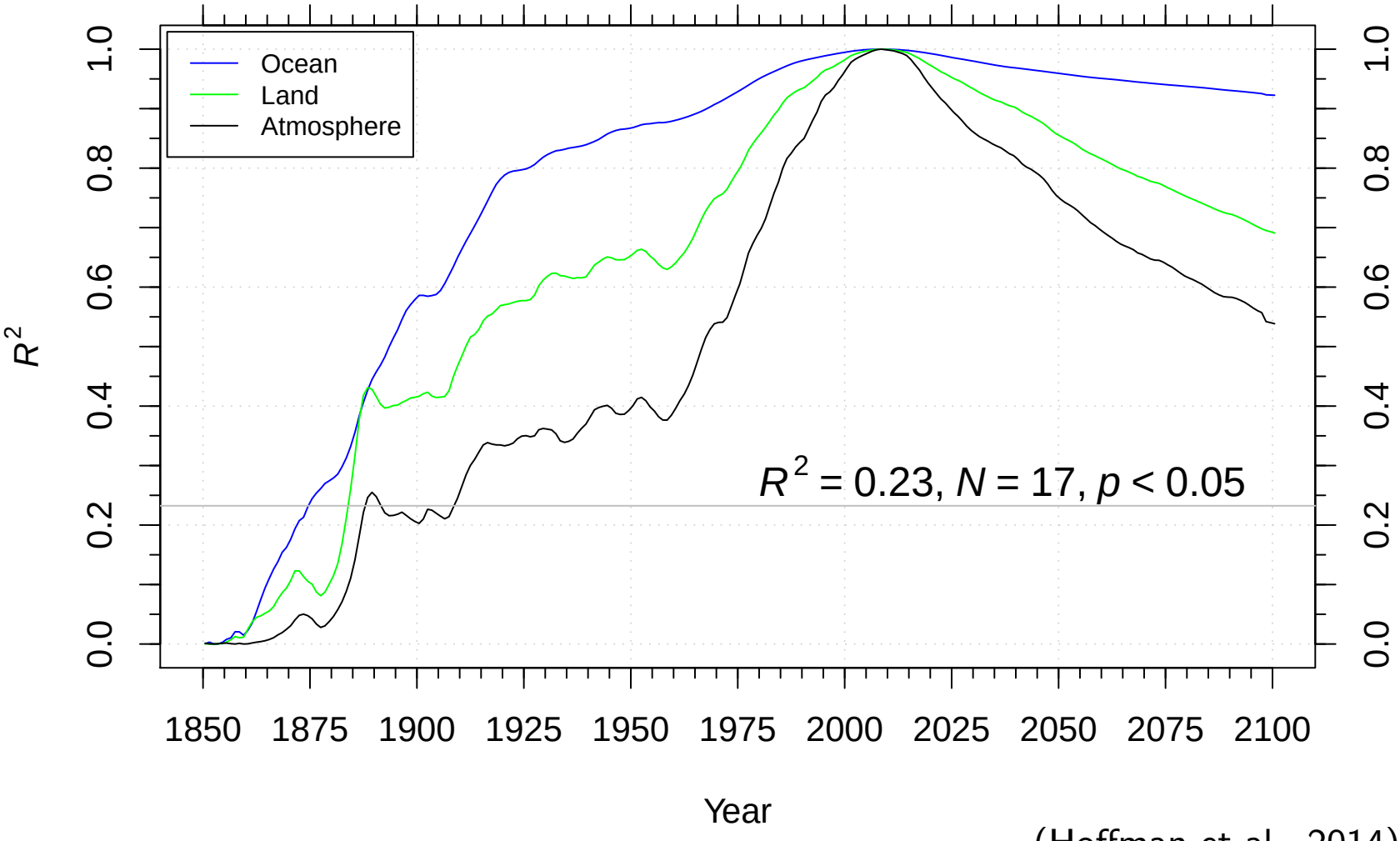

(Hoffman et al., 2014)

The coefficients of determination (R^2) of the multi-model bias structure relative to the set of CMIP5 model atmospheric CO_2, and ocean and land carbon predictions for 2010 are statistically significant for 1910–2100.

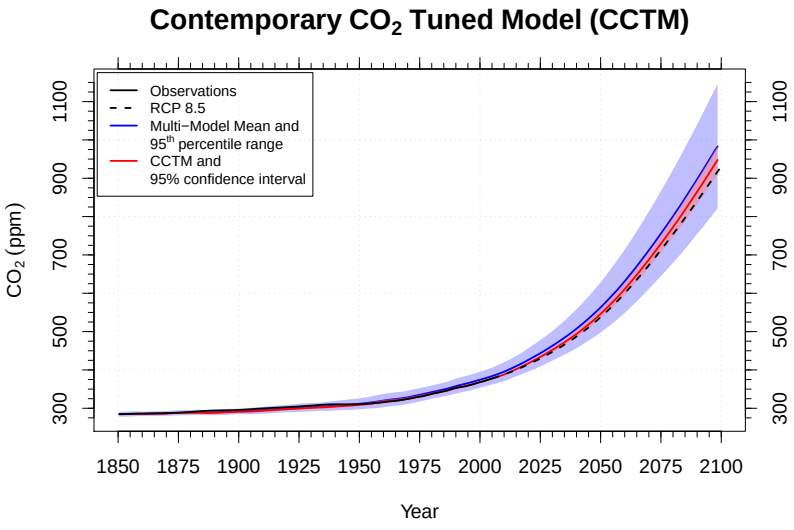

We used this regression to create a contemporary CO_2 tuned model (CCTM) estimate of the atmospheric CO_2 trajectory for the 21st century.

The width of the probability density is much smaller for the CCTM, by almost a factor of 6 at 2060 and almost a factor of 5 at 2100, indicating a significant reduction in the range of uncertainty for the CCTM prediction.

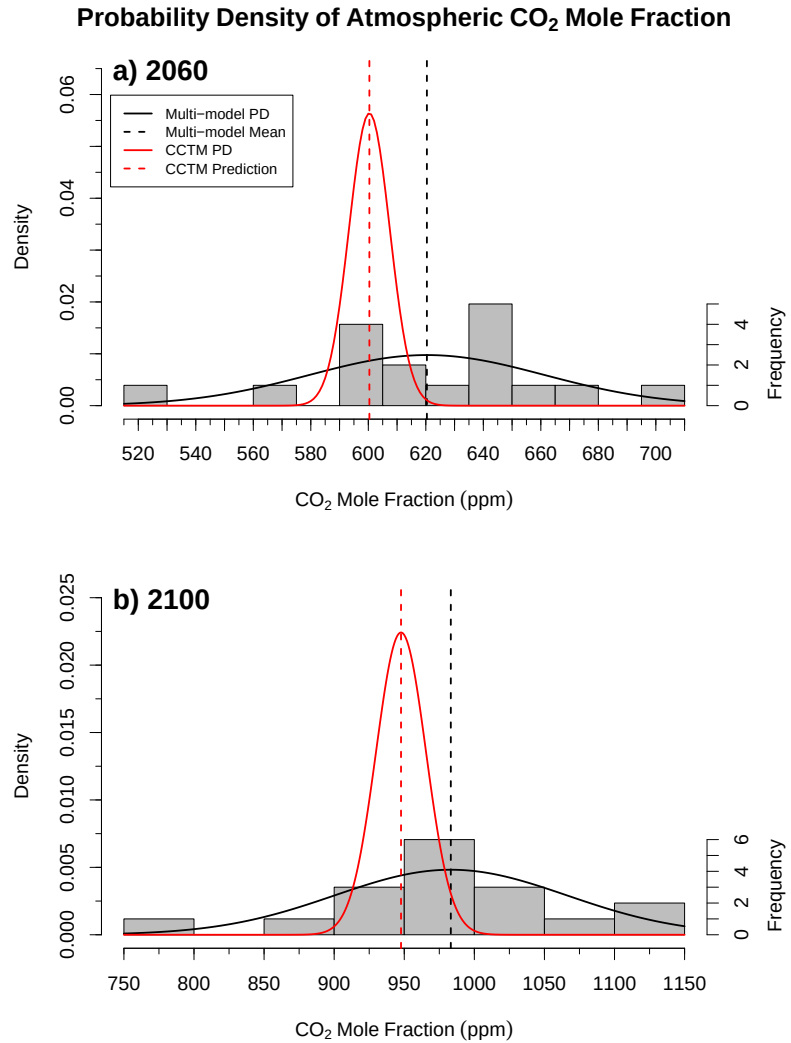

Best estimate tuned using Mauna Loa CO_2 data:

At 2060: 600 ± 14 ppm, 21 ppm below the multi-model mean

At 2100: 947 ± 35 ppm, 32 ppm below the multi-model mean

(Hoffman et al., 2014)

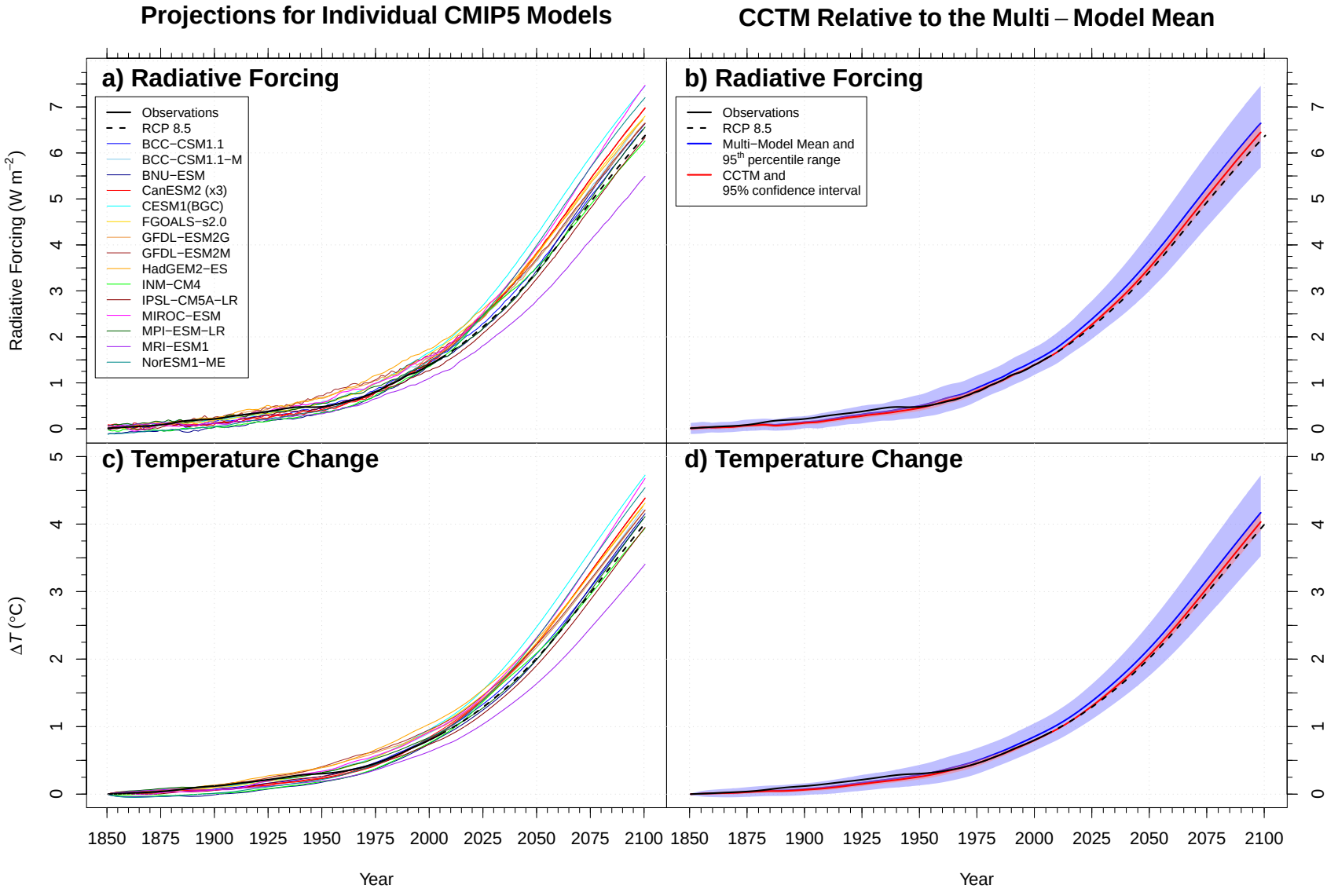

(Hoffman et al., 2014)

We calculated the CO_2 radiative forcing and used an impulse response function (tuned to the mean transient climate response of CMIP5 models) to equitably compute the resulting temperature change for models and the CCTM. At 2100, the CCTM $\Delta T = 4.0 \pm 0.1^{\circ}$C, while the multi-model mean $\Delta T = 4.2 \pm 0.6^{\circ}$C.

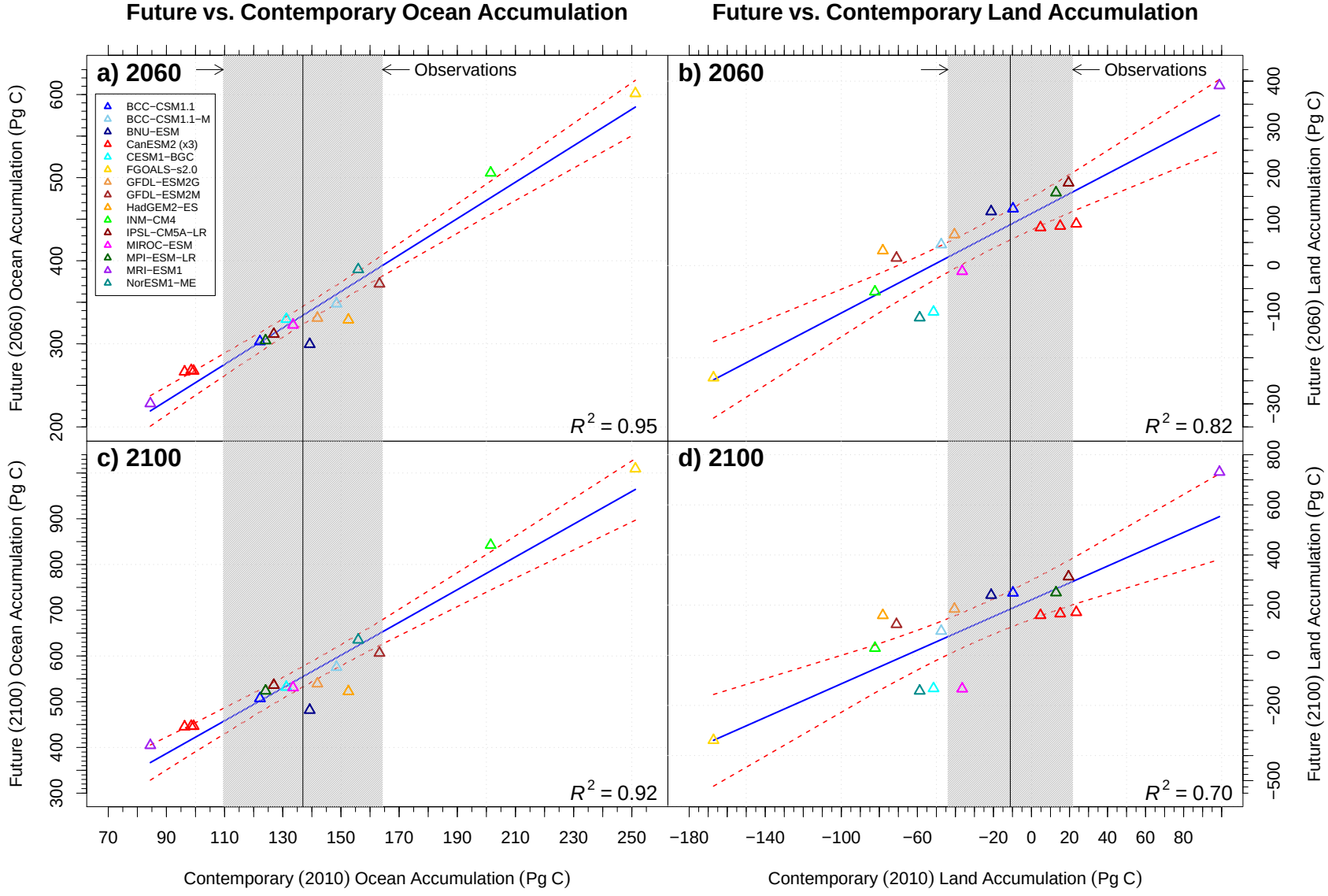

(Hoffman et al., 2014)

We also developed a multi-model constraint on the evolution of ocean and land anthropogenic inventories. Since observational uncertainties are higher for ocean and land, uncertainties in future estimates cannot be reduced as much as for atmospheric CO_2.

Conclusions

- A considerable amount of the model-to-model variability of CO_2 in the 21st century can be traced to biases that exist at the end of the observational record.
- Bias persistence was highest for the ocean, followed by land, and then by the atmosphere.
- Carbon cycle biases are likely primarily linked with concentration–carbon feedback processes:
  - ocean – Southern Ocean overturning, vertical mixing processes
  - land – CO_2 fertilization, allocation to woody pools, nutrient limitation
- Future fossil fuel emissions targets designed to stabilize CO_2 levels would be too low if estimated from the multi-model mean of ESMs.
  - ESMs overestimate contemporary CO_2 with observed emissions.
- Models could be improved through extensive comparison with observations and community model benchmarking.

For more information, see also Poster #77 in Room 20

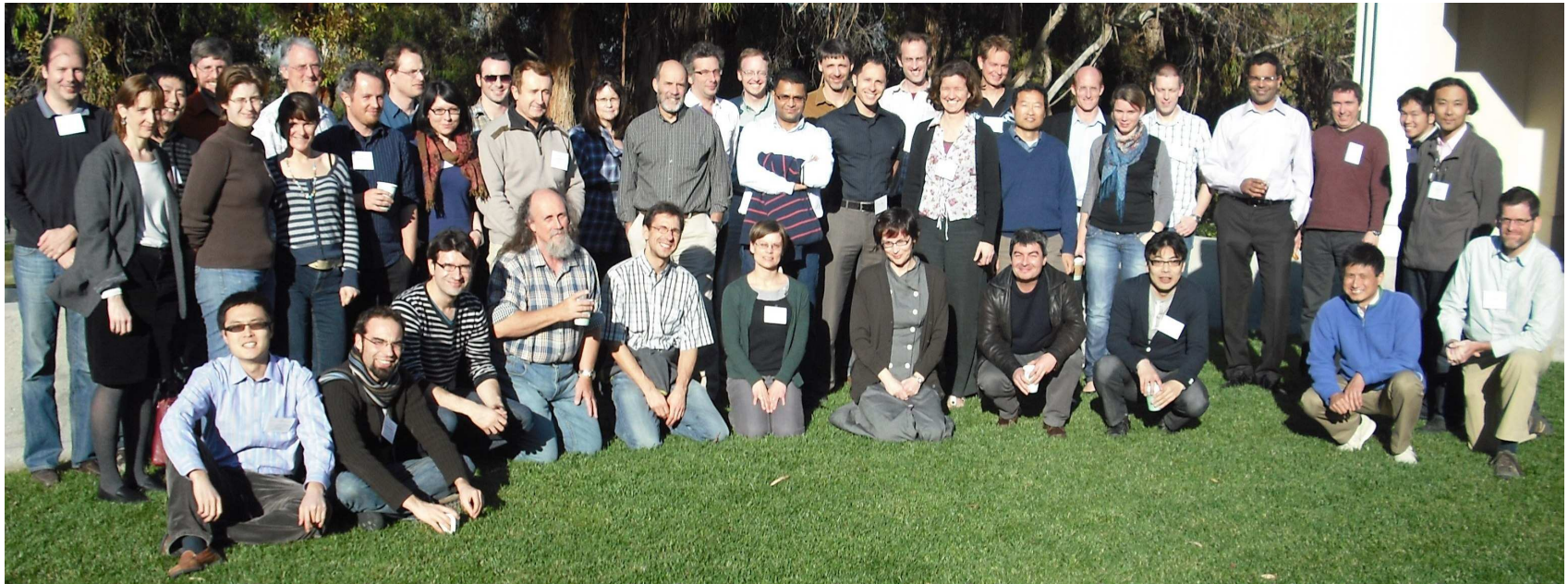

- We co-organized inaugural meeting and ∼45 researchers participated from the United States, Canada, the United Kingdom, the Netherlands, France, Germany, Switzerland, China, Japan, and Australia.
- **ILAMB Goals:** Develop internationally accepted benchmarks for model performance, advocate for design of open-source software system, and strengthen linkages between experimental, monitoring, remote sensing, and climate modeling communities. *Initial focus on CMIP5 models.*
- Provides methodology for model–data comparison and baseline standard for performance of land model process representations (Luo et al., 2012).

ILAMB 1.0 Benchmarks Now Under Development

	Annual Mean	Seasonal Cycle	Interannual Variability	Trend	Data Source
Atmospheric CO_2					
Flask/conc. + transport		✓	✓	✓	NOAA, SIO, CSIRO
TCCON + transport		✓	✓	✓	Caltech
Fluxnet					
GPP, NEE, TER, LE, H, RN	✓	✓	✓		Fluxnet, MAST-DC
Gridded: GPP	✓	✓	?		MPI-BGC
Hydrology/Energy					
runoff ratio (R/P) ~~river flow~~	✓		✓		GRDC, Dai, GFDL
global runoff/ocean balance	✓				Syed/Famiglietti
albedo (multi-band)		✓	✓		MODIS, CERES
soil moisture		✓	✓		de Jeur, SMAP
column water		✓	✓		GRACE
snow cover	✓	✓	✓	✓	AVHRR, GlobSnow
snow depth/SWE	✓	✓	✓	✓	CMC (N. America)
T_{air} & P	✓	✓	✓	✓	CRU, GPCP and TRMM
Gridded: LE, H	✓	✓			MPI-BGC, dedicated ET
Ecosystem Processes & State					
soil C, N	✓				HWSD, MPI-BGC
litter C, N	✓				LIDET
soil respiration	✓	✓	✓	✓	Bond-Lamberty
FAPAR	✓	✓			MODIS, SeaWIFS
biomass & change	✓			✓	Saatchi, Pan, Blackard
canopy height	✓				Lefsky, Fisher
NPP	✓				EMDI, Luyssaert
Vegetation Dynamics					
fire — burned area	✓	✓	✓		GFED3
wood harvest	✓			✓	Hurtt
land cover	✓				MODIS PFT fraction

Example Benchmark Score Sheet from C-LAMP

Models →

BGC Datasets ↓

Metric	Metric components	Uncertainty of obs.	Scaling mismatch	Total score	Sub-score	CASA′		CN	
LAI	Matching MODIS observations			15.0		13.5		12.0	
	• Phase (assessed using the month of maximum LAI)	Low	Low		6.0		5.1		4.2
	• Maximum (derived separately for major biome classes)	Moderate	Low		5.0		4.6		4.3
	• Mean (derived separately for major biome classes)	Moderate	Low		4.0		3.8		3.5
NPP	Comparisons with field observations and satellite products			10.0		8.0		8.2	
	• Matching EMDI Net Primary Production observations	High	High		2.0		1.5		1.6
	• EMDI comparison, normalized by precipitation	Moderate	Moderate		4.0		3.0		3.4
	• Correlation with MODIS (r^2)	High	Low		2.0		1.6		1.4
	• Latitudinal profile comparison with MODIS (r^2)	High	Low		2.0		1.9		1.8
CO_2 annual cycle	Matching phase and amplitude at Globalview flash sites			15.0		10.4		7.7	
	• 60°–90°N	Low	Low		6.0		4.1		2.8
	• 30°–60°N	Low	Low		6.0		4.2		3.2
	• 0°–30°N	Moderate	Low		3.0		2.1		1.7
Energy & CO_2 fluxes	Matching eddy covariance monthly mean observations			30.0		17.2		16.6	
	• Net ecosystem exchange	Low	High		6.0		2.5		2.1
	• Gross primary production	Moderate	Moderate		6.0		3.4		3.5
	• Latent heat	Low	Moderate		9.0		6.4		6.4
	• Sensible heat	Low	Moderate		9.0		4.9		4.6
Transient dynamics	Evaluating model processes that regulate carbon exchange on decadal to century timescales			30.0		16.8		13.8	
	• Aboveground live biomass within the Amazon Basin	Moderate	Moderate		10.0		5.3		5.0
	• Sensitivity of NPP to elevated levels of CO_2: comparison to temperate forest FACE sites	Low	Moderate		10.0		7.9		4.1
	• Interannual variability of global carbon fluxes: comparison with TRANSCOM	High	Low		5.0		3.6		3.0
	• Regional and global fire emissions: comparison to GFEDv2	High	Low		5.0		0.0		1.7
			Total:	**100.0**		**65.9**		**58.3**	

(Randerson et al., 2009)

10 Alaska Ecoregions, Present and Future

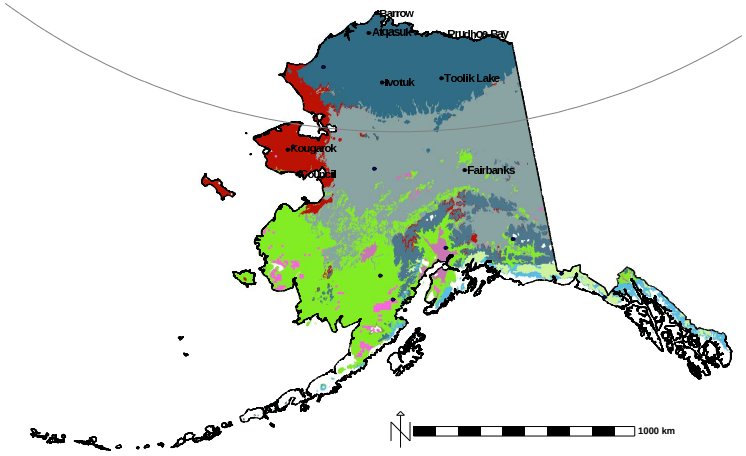

2000–2009

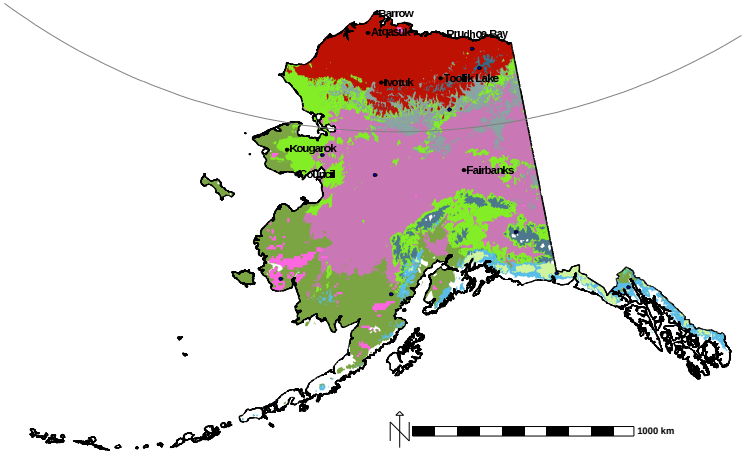

2090–2099

(Hoffman et al., 2013)

Since the random colors are the same in both maps, a change in color represents an environmental change between the present and the future.

At this level of division, the conditions in the large boreal forest become compressed onto the Brooks Range and the conditions on the Seward Peninsula "migrate" to the North Slope.

Present Representativeness of Barrow or "Barrow-ness"

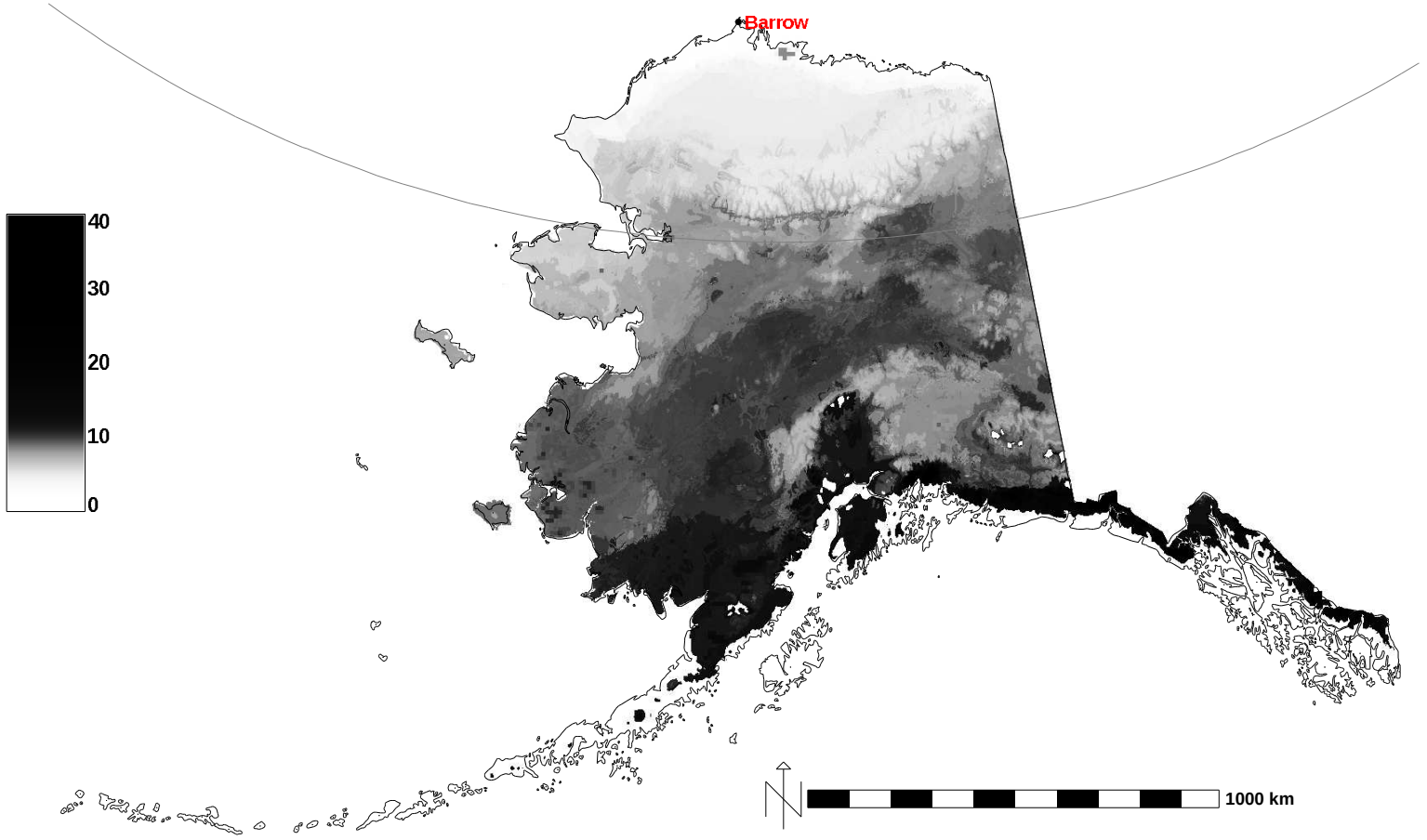

(Hoffman et al., 2013)

Light-colored regions are well represented and dark-colored regions are poorly represented by the sampling location listed in **red**.

Network Representativeness: Barrow + Council

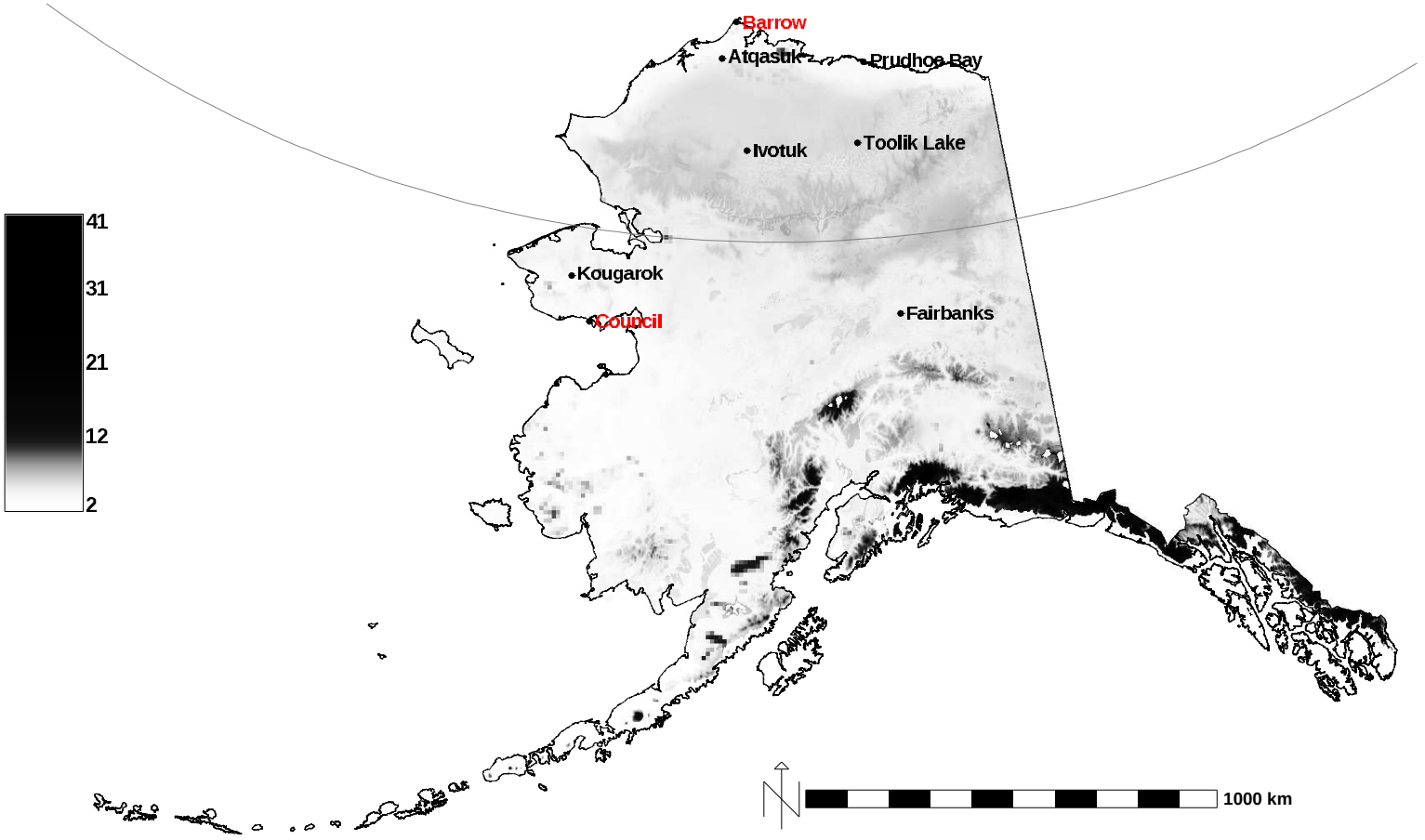

(Hoffman et al., 2013)

Light-colored regions are well represented and dark-colored regions are poorly represented by the sampling location listed in **red**.

Barrow Environmental Observatory (BEO)

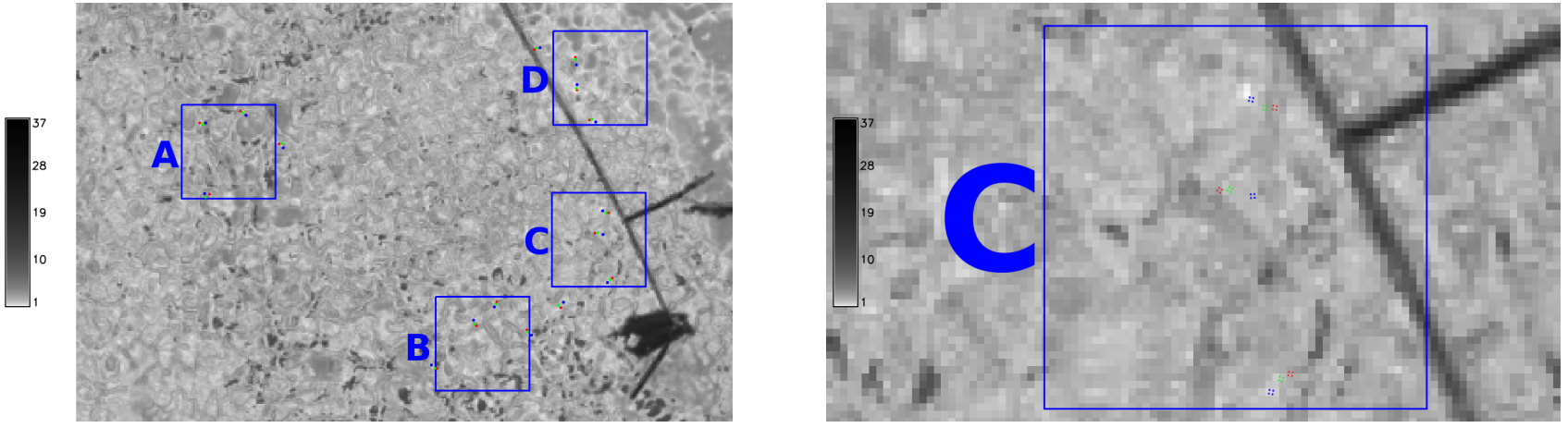

(Kumar et al., in prep)

Representativeness map for vegetation sampling points for A, B, C, and D sampling area (left) and zoomed in on the C samping area (right) developed from WorldView2 satellite images for the year 2010 and LiDAR data.

Vegetation sampling locations represent polygon troughs (red), edges (green), and centers (blue).

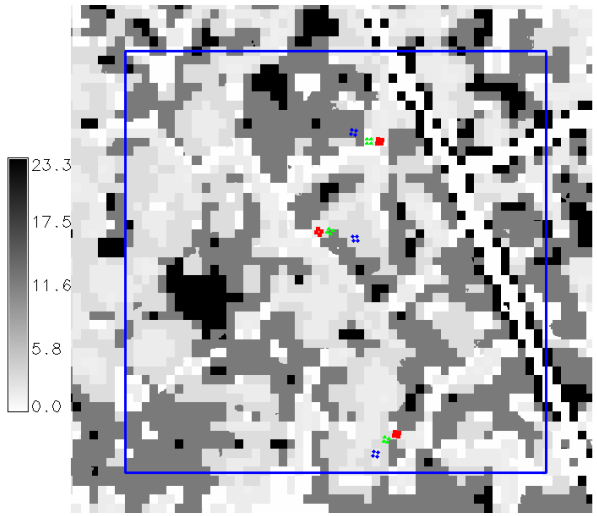

(a) dry tundra gramanoid

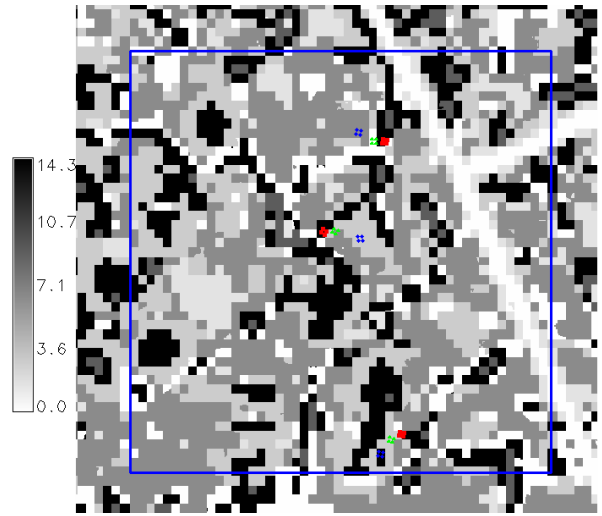

(b) forb

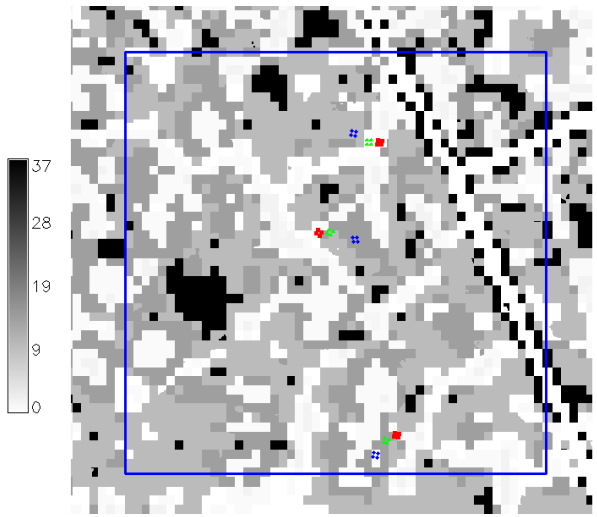

(c) lichen

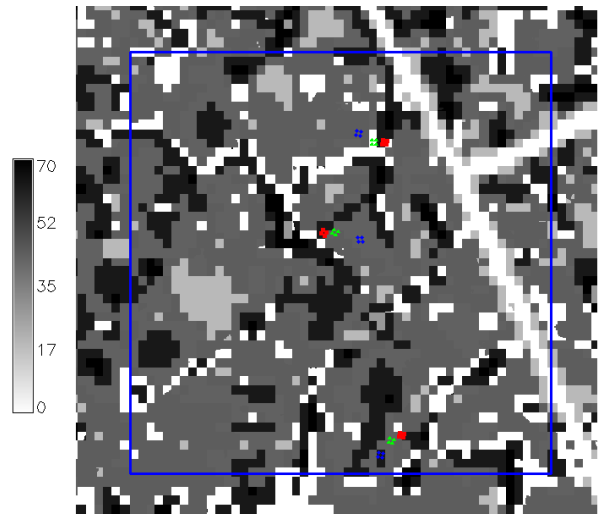

(d) moss

(Kumar et al., in prep)

Example plant functional type (PFT) distributions scaled up from vegetation sampling locations.

Triple-network Global Representativeness

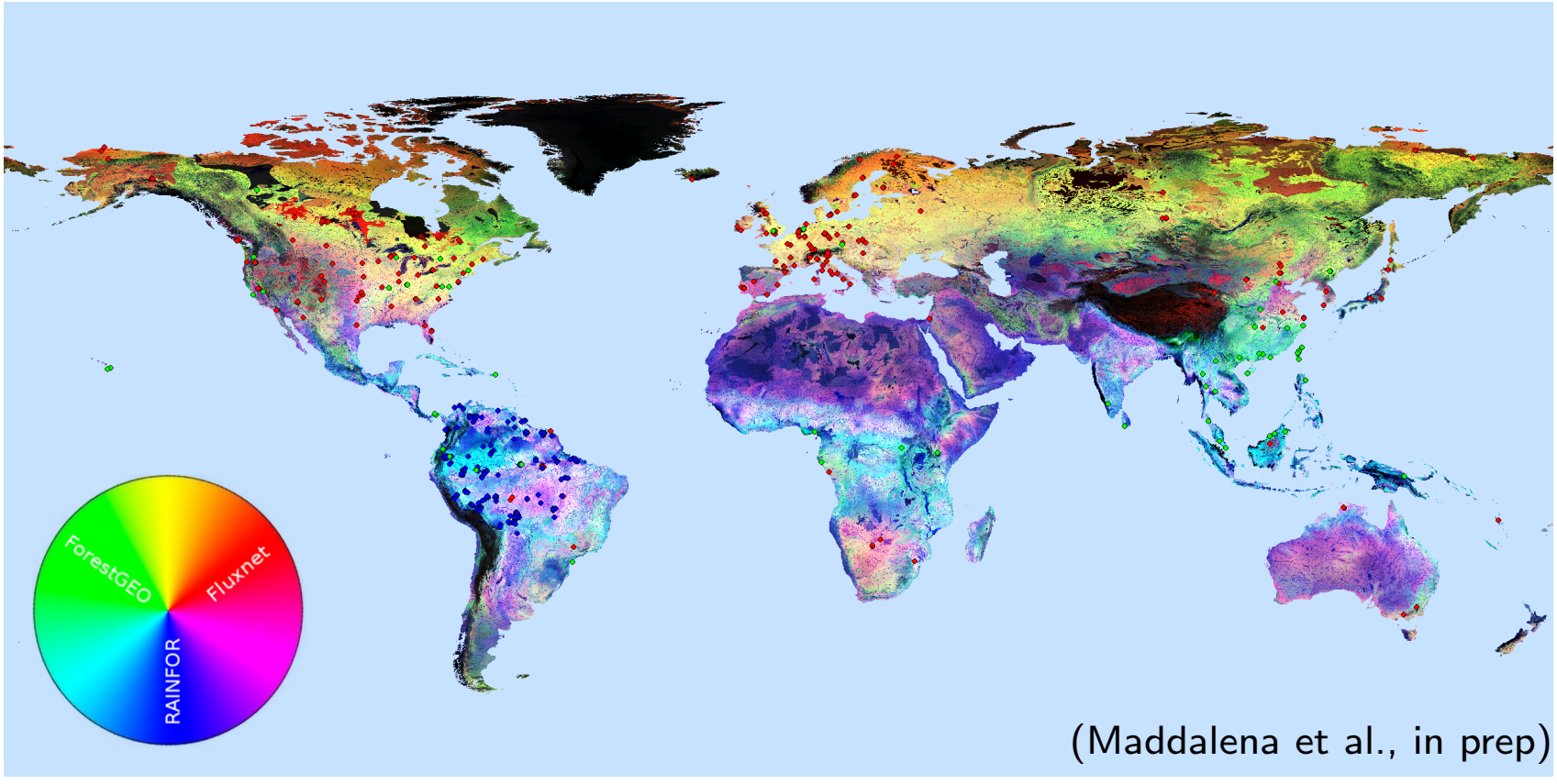

Map indicates which sampling network offers the most representative coverage at any location. Every location is made up of a combination of three primary colors from Fluxnet (red), ForestGEO (green), and RAINFOR (blue).

CESD Mission – My view

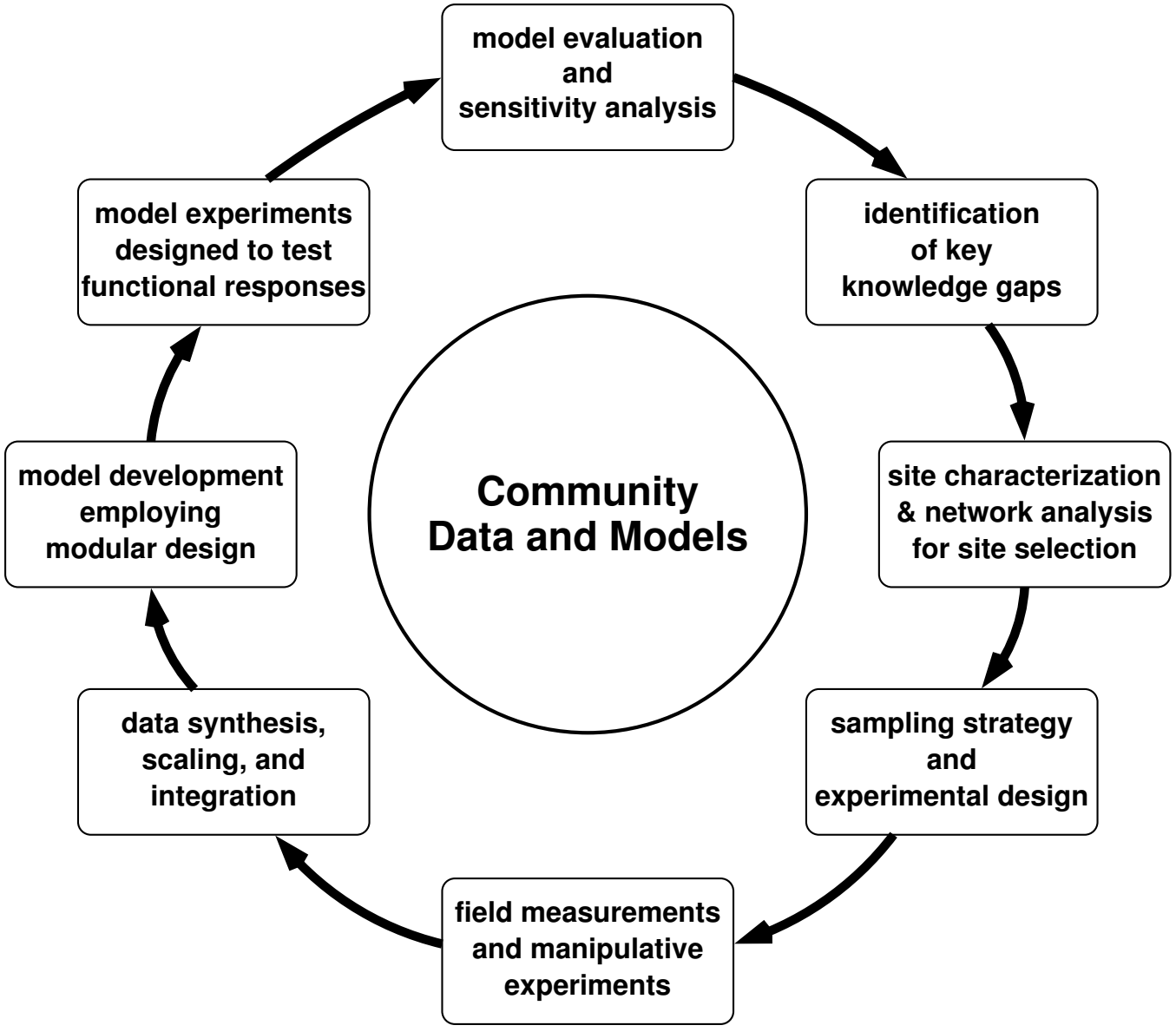

CESD Mission – My view

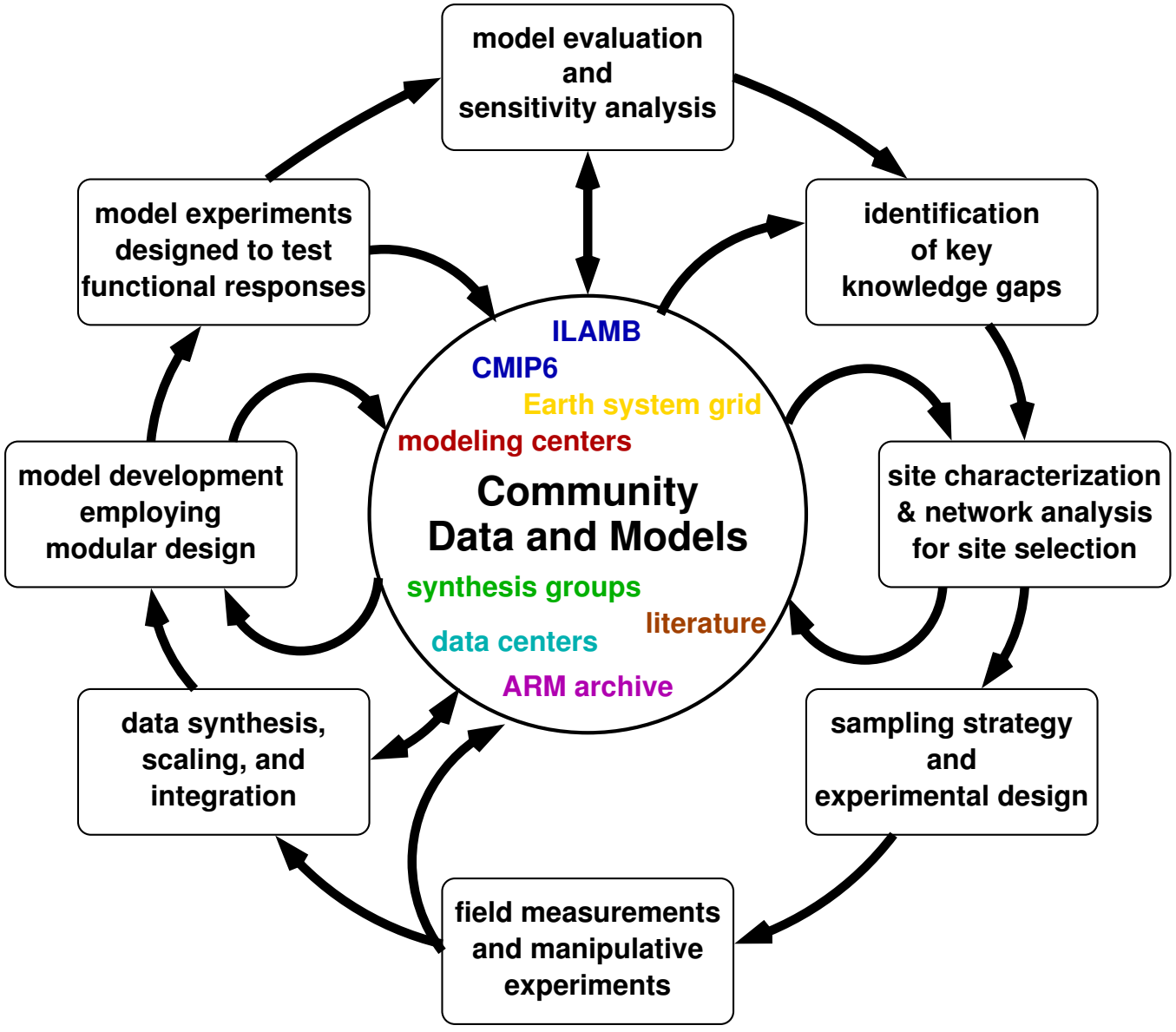

CESD Mission – My view

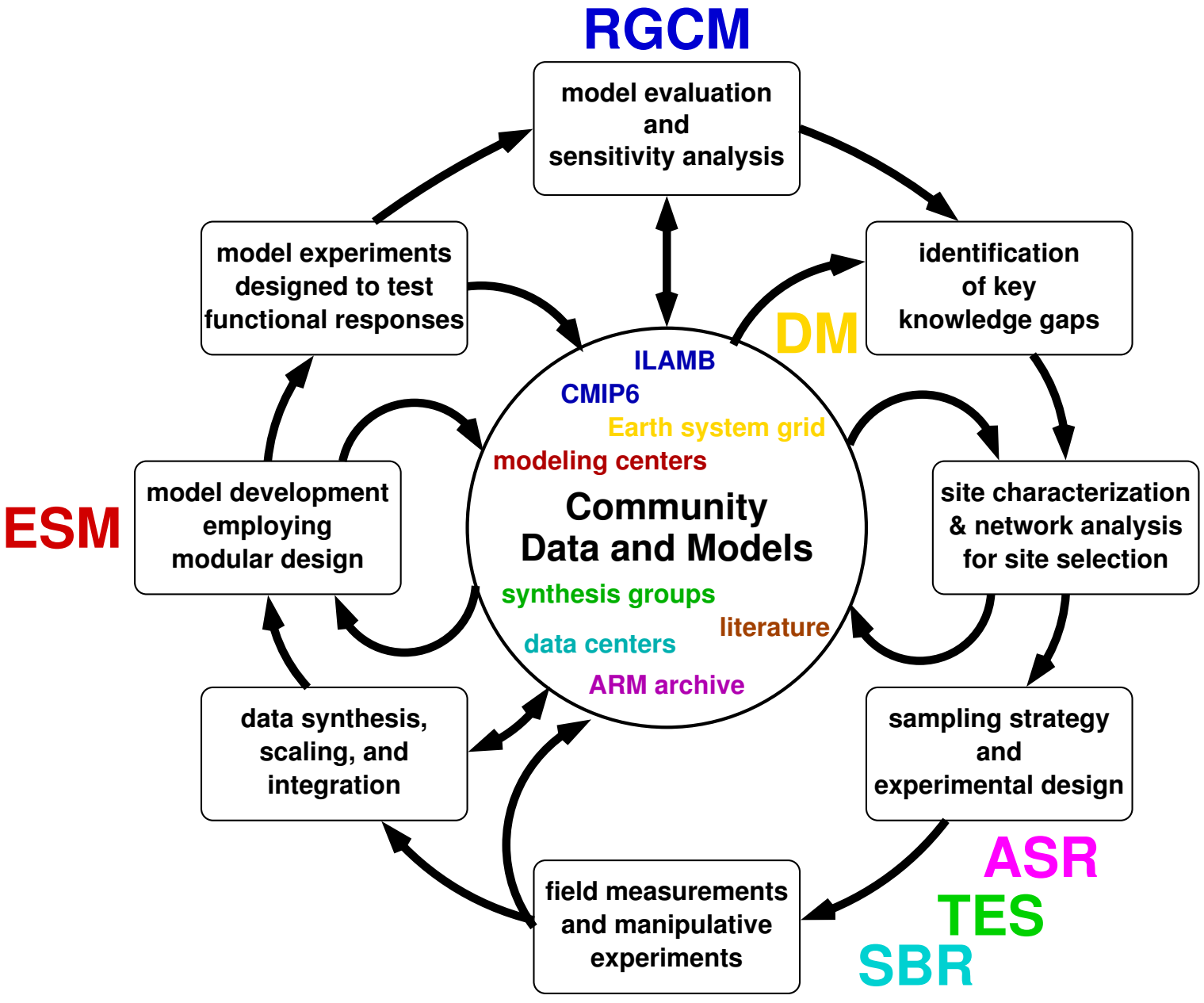

Biogeochemistry–Climate System Feedbacks

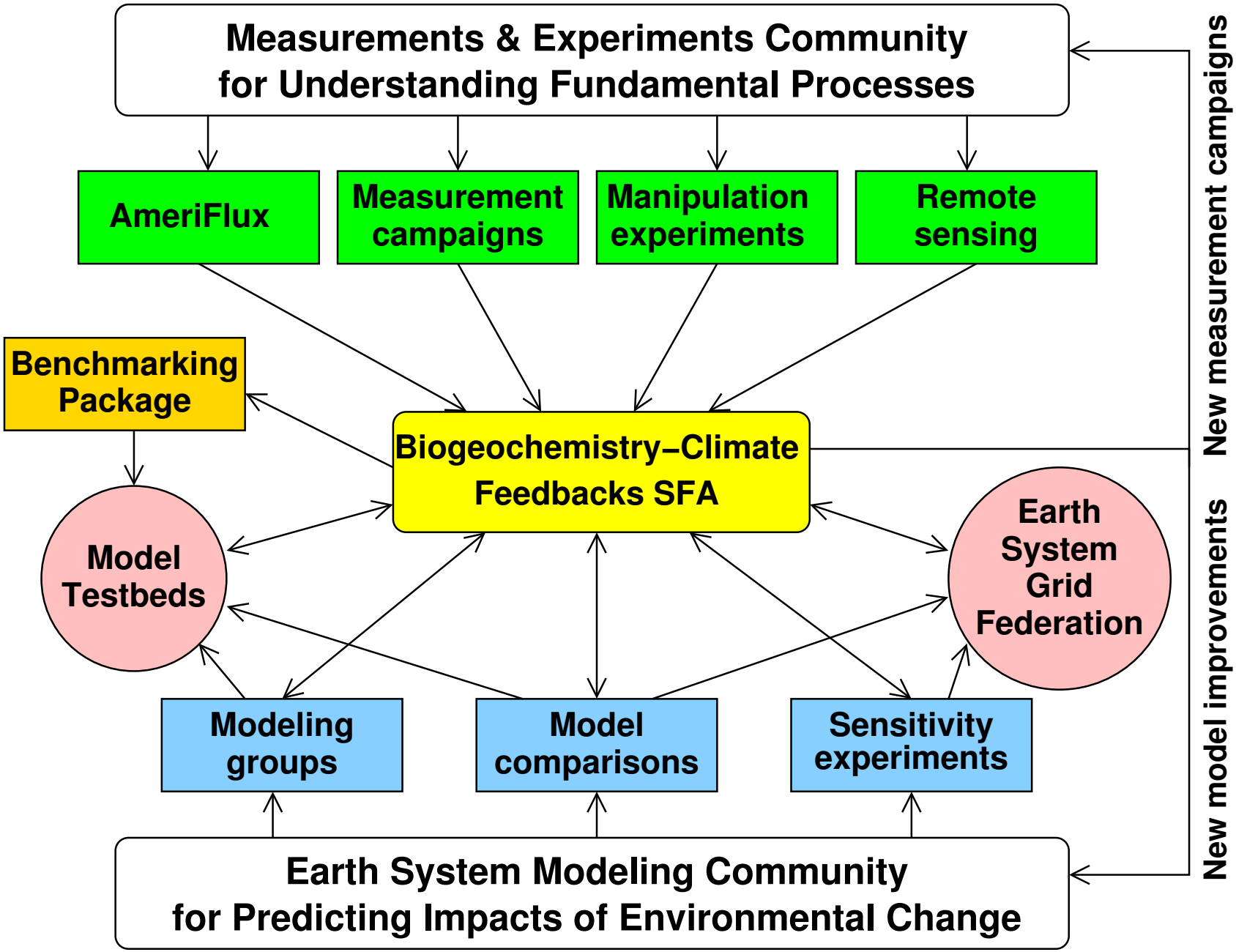

Take Home Message from Bruce and Forrest

- **Modelers:** Confront models with data. *Just like voting, do this early and often!*
  - Make model evaluation tools and data free and open, facilitating community contributions. *It takes a village!*
  - Design model experiments and analyses to identify weaknesses and inspire new measurements.
- **Data Gatherers:** Make data available early and characterize and report all measurement uncertainties.
  - Confront the environment with new sensors, drones, and aerial and space-based instrumentation to answer key questions about mechanisms.
  - Conduct measurements to improve our understanding of processes and inform model development.
- **Integrated Assessors:** Creatively employ multi-model projections and use results of model evalutaion as a lens through which to view predictions of the future.

Acknowledgments

U.S. DEPARTMENT OF ENERGY

Office of Science

This research was sponsored by the Climate and Environmental Sciences Division (CESD) of the Biological and Environmental Research (BER) Program in the U. S. Department of Energy Office of Science and the National Science Foundation (AGS-1048890). This research used resources of the National Center for Computational Sciences (NCCS) at Oak Ridge National Laboratory (ORNL), which is managed by UT-Battelle, LLC, for the U. S. Department of Energy under Contract No. DE-AC05-00OR22725.

We acknowledge the World Climate Research Programme's Working Group on Coupled Modelling, which is responsible for CMIP, and we thank the climate modeling groups for producing and making available their model output. For CMIP the U. S. Department of Energy's Program for Climate Model Diagnosis and Intercomparison provides coordinating support and led development of software infrastructure in partnership with the Global Organization for Earth System Science Portals.

References

R. J. Andres, J. S. Gregg, L. Losey, G. Marland, and T. A. Boden. Monthly, global emissions of carbon dioxide from fossil fuel consumption. *Tellus B*, 63(3):309–327, July 2011. doi: 10.1111/j.1600-0889.2011.00530.x.

P. M. Cox, D. Pearson, B. B. Booth, P. Friedlingstein, C. Huntingford, C. D. Jones, and C. M. Luke. Sensitivity of tropical carbon to climate change constrained by carbon dioxide variability. *Nature*, 494(7437):341–344, Feb. 2013. doi: 10.1038/nature11882.

A. Hall and X. Qu. Using the current seasonal cycle to constrain snow albedo feedback in future climate change. *Geophys. Res. Lett.*, 33(3):L03502, Feb. 2006. doi: 10.1029/2005GL025127.

F. M. Hoffman, J. Kumar, R. T. Mills, and W. W. Hargrove. Representativeness-based sampling network design for the State of Alaska. *Landscape Ecol.*, 28(8):1567–1586, Oct. 2013. doi: 10.1007/s10980-013-9902-0.

F. M. Hoffman, J. T. Randerson, V. K. Arora, Q. Bao, P. Cadule, D. Ji, C. D. Jones, M. Kawamiya, S. Khatiwala, K. Lindsay, A. Obata, E. Shevliakova, K. D. Six, J. F. Tjiputra, E. M. Volodin, and T. Wu. Causes and implications of persistent atmospheric carbon dioxide biases in Earth System Models. *J. Geophys. Res. Biogeosci.*, 119(2):141–162, Feb. 2014. doi: 10.1002/2013JG002381.

S. Khatiwala, T. Tanhua, S. Mikaloff Fletcher, M. Gerber, S. C. Doney, H. D. Graven, N. Gruber, G. A. McKinley, A. Murata, A. F. Ríos, and C. L. Sabine. Global ocean storage of anthropogenic carbon. *Biogeosci.*, 10(4): 2169–2191, Apr. 2013. doi: 10.5194/bg-10-2169-2013.

Y. Q. Luo, J. T. Randerson, G. Abramowitz, C. Bacour, E. Blyth, N. Carvalhais, P. Ciais, D. Dalmonech, J. B. Fisher, R. Fisher, P. Friedlingstein, K. Hibbard, F. Hoffman, D. Huntzinger, C. D. Jones, C. Koven, D. Lawrence, D. J. Li, M. Mahecha, S. L. Niu, R. Norby, S. L. Piao, X. Qi, P. Peylin, I. C. Prentice, W. Riley, M. Reichstein, C. Schwalm, Y. P. Wang, J. Y. Xia, S. Zaehle, and X. H. Zhou. A framework for benchmarking land models. *Biogeosci.*, 9(10):3857–3874, Oct. 2012. doi: 10.5194/bg-9-3857-2012.

M. Meinshausen, S. Smith, K. Calvin, J. Daniel, M. Kainuma, J.-F. Lamarque, K. Matsumoto, S. Montzka, S. Raper, K. Riahi, A. Thomson, G. Velders, and D. P. van Vuuren. The RCP greenhouse gas concentrations and their extensions from 1765 to 2300. *Clim. Change*, 109(1):213–241, Nov. 2011. doi: 10.1007/s10584-011-0156-z.

J. T. Randerson, F. M. Hoffman, P. E. Thornton, N. M. Mahowald, K. Lindsay, Y.-H. Lee, C. D. Nevison, S. C. Doney, G. Bonan, R. Stöckli, C. Covey, S. W. Running, and I. Y. Fung. Systematic assessment of terrestrial biogeochemistry in coupled climate-carbon models. *Global Change Biol.*, 15(9):2462–2484, Sept. 2009. doi: 10.1111/j.1365-2486.2009.01912.x.

C. L. Sabine, R. A. Feely, N. Gruber, R. M. Key, K. Lee, J. L. Bullister, R. Wanninkhof, C. S. Wong, D. W. R. Wallace, B. Tilbrook, F. J. Millero, T.-H. Peng, A. Kozyr, T. Ono, and A. F. Rios. The oceanic sink for anthropogenic CO_2. *Science*, 305(5682):367–371, July 2004. doi: 10.1126/science.1097403.

Extra Slides

Model inventory comparison with Sabine et al. (2004)

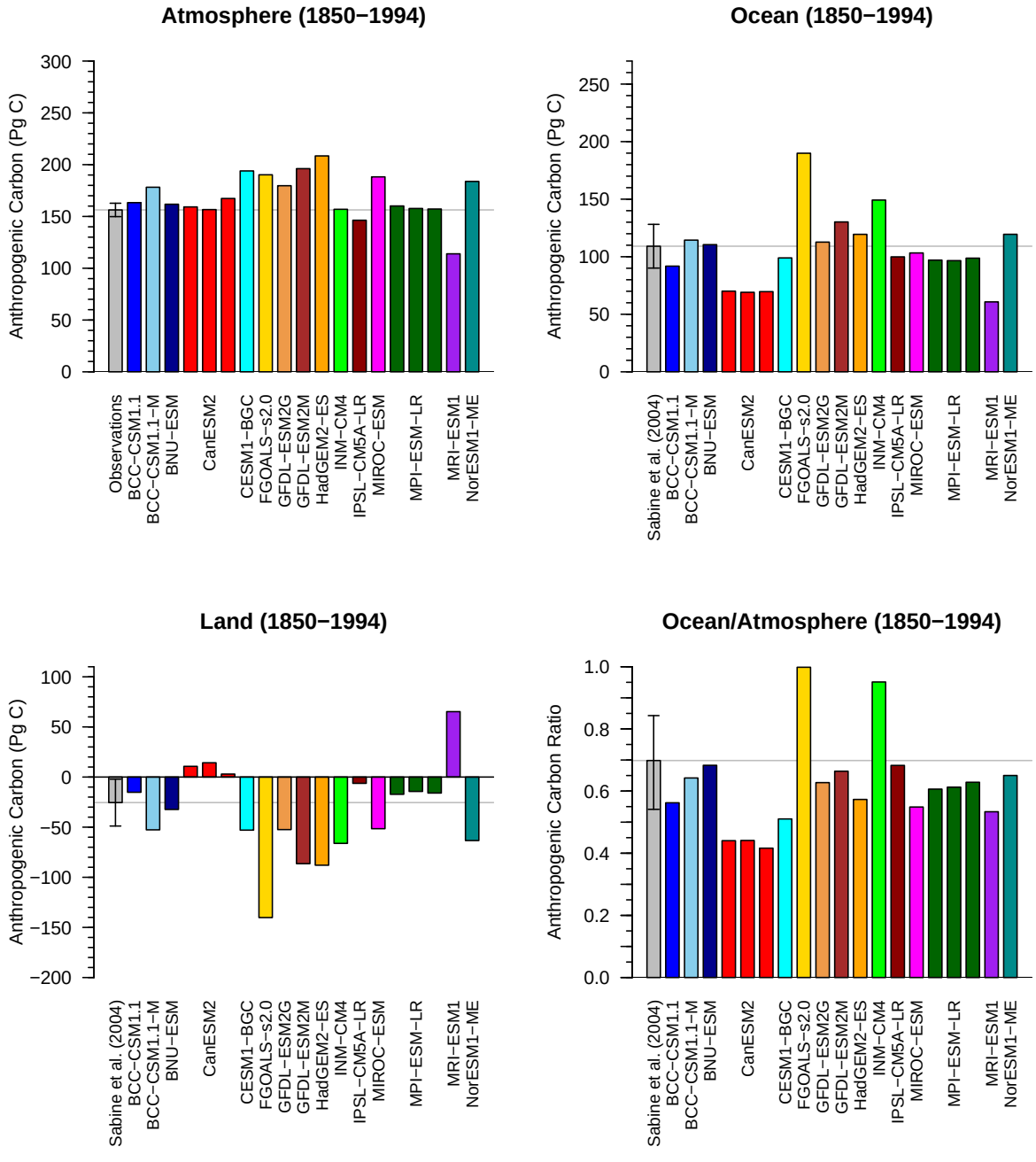

Implications for CO_2, Radiative Forcing, and Temperature

Model	CO_2 Mole Fraction (ppm)			Radiative Forcing ($W\,m^{-2}$)			Cumulative ΔT (°C)			ΔT Bias (°C)		
	2010	2060	2100	2010	2060	2100	2010	2060	2100	2010	2060	2100
BCC-CSM1.1	390	603	945	1.70	4.03	6.43	0.97	2.39	4.02	0.03	0.02	−0.01
BCC-CSM1.1-M	396	619	985	1.78	4.16	6.65	1.04	2.49	4.16	0.10	0.12	0.13
BNU-ESM	382	602	963	1.59	4.02	6.53	0.90	2.33	4.07	−0.04	−0.04	0.04
CanESM2 r1	394	641	1024	1.75	4.36	6.86	0.98	2.58	4.30	0.04	0.21	0.27
CanESM2 r2	392	641	1023	1.72	4.35	6.85	0.98	2.57	4.30	0.04	0.20	0.27
CanESM2 r3	396	641	1025	1.78	4.35	6.87	1.01	2.58	4.30	0.07	0.21	0.27
CESM1-BGC	407	697	1121	1.92	4.80	7.34	1.12	2.85	4.64	0.18	0.48	0.61
FGOALS-s2.0	404	636	993	1.89	4.31	6.70	1.09	2.57	4.23	0.15	0.20	0.20
GFDL-ESM2G	395	616	967	1.77	4.14	6.56	1.04	2.49	4.12	0.10	0.12	0.09
GFDL-ESM2M	400	621	964	1.83	4.18	6.54	1.09	2.52	4.13	0.15	0.15	0.10
HadGEM2-ES	411	636	983	1.98	4.31	6.64	1.18	2.60	4.20	0.24	0.23	0.17
INM-CM4	386	591	897	1.64	3.92	6.15	0.92	2.36	3.86	−0.02	−0.01	−0.17
IPSL-CM5A-LR	375	573	908	1.48	3.75	6.22	0.86	2.21	3.87	−0.08	−0.16	−0.16
MIROC-ESM	398	658	1121	1.81	4.50	7.35	1.06	2.67	4.58	0.12	0.30	0.55
MPI-ESM-LR r1	383	590	948	1.60	3.91	6.45	0.95	2.31	4.03	0.01	−0.06	0.00
MRI-ESM1	361	516	778	1.28	3.20	5.39	0.74	1.89	3.33	−0.20	−0.48	−0.70
NorESM1-ME	391	667	1070	1.72	4.57	7.09	0.98	2.68	4.46	0.04	0.31	0.43
Multi-model Mean	392	621	980	1.72	4.18	6.63	1.00	2.48	4.17	0.06	0.11	0.14
CCTM Estimate	385	600	948	1.62	4.01	6.45	0.94	2.37	4.03	—	—	—
Historical + RCP 8.5	385	590	917	1.63	3.91	6.27	0.94	2.32	3.93	0.00	−0.05	−0.10